

MAASS FORMS AND THEIR L-FUNCTIONS

DAVID W. FARMER AND STEFAN LEMURELL

Abstract. We present examples of Maass forms on Hecke congruence groups, giving low eigenvalues on $\Gamma_0(p)$ for small prime p , and the first 1000 eigenvalues for $\Gamma_0(11)$. We also present calculations of the L-functions associated to the Maass forms and make comparisons to the predictions from random matrix theory.

1. Introduction

Much recent progress in understanding L-functions has come from the idea of a "family" of L-functions with an associated symmetry type [5]. The idea is that to a naturally occurring collection of L-functions one can associate a classical compact group: unitary, symplectic, or orthogonal. One expects the analytic properties of the L-functions to be largely governed by the symmetry type. This philosophy has produced a wealth of interesting predictions which have been confirmed both theoretically and numerically. See [1] for an extensive discussion.

The family of L-functions of interest to us here is the collection of L-functions associated to Maass forms. Specifically, for a given Hecke congruence group $\Gamma_0(N)$, we consider the Maass forms on $\Gamma_0(N)$ and the L-functions associated to those Maass forms. This constitutes an "orthogonal" family of L-functions, and this leads to some specific predictions about statistical properties of the critical values and the zeros of the L-functions. In this paper we provide the first numerical tests of these predictions by finding the first 1000 new form Maass forms on $\Gamma_0(11)$ and computing the associated L-functions. We also test standard predictions about the statistics of those eigenvalues, and we find the first few eigenvalues on $\Gamma_0(p)$ for small p .

In the next section we recall properties of Maass forms and their associated L-functions. In section 3 we describe our algorithm for locating and computing Maass forms. We then present the results of our calculations, in section 4 addressing the low eigenvalues on $\Gamma_0(p)$, and in section 5 the first 1000 eigenvalues for $\Gamma_0(11)$. In section 6 we give example plots of Maass L-functions and discuss their general features. In section 7 we compare the random matrix predictions to our L-function data. Finally, in section 8 we describe how the L-functions were computed.

2. Maass forms and their L-Functions

The L-functions we consider are obtained from Maass forms on the Hecke congruence group $\Gamma_0(11)$. We first recall the definition of Maass form, and then describe the connection with L-functions. A good reference on Maass forms is Iwaniec's book [4].

Research of the first author supported by the American Institute of Mathematics and the NSF Focused Research Group grant DMS 0244660. Research of the second author supported in part by "Stiftelsen för internationalisering av högskoleutbildning och forskning" (STINT).

2.1. **Maass forms.** A Maass form on a group $\mathrm{PSL}(2; \mathbb{R})$ is a function $f : \mathbb{H} \rightarrow \mathbb{R}$ which satisfies:

- (1.1) $f(\gamma z) = f(z)$ for all $\gamma \in \mathrm{PSL}(2; \mathbb{R})$,
- (1.2) f vanishes at the cusps of \mathbb{H} , and
- (1.3) $\Delta f = \lambda f$ for some $\lambda > 0$,

where

$$\Delta = Y^2 \left(\frac{\partial^2}{\partial X^2} + \frac{\partial^2}{\partial Y^2} \right)$$

is the Laplace-Beltrami operator on \mathbb{H} . We set $\mathbb{H} = \frac{1}{4} + \mathbb{R}^2$.

In number theory, Maass forms most commonly arise on Hecke congruence groups:

$$\Gamma_0(N) = \left\{ \begin{pmatrix} a & b \\ c & d \end{pmatrix} \in \mathrm{PSL}(2; \mathbb{Z}) : N \mid c \right\}$$

Here we consider new forms on $\Gamma_0(N)$. This implies that

$$(2.1) \quad f(z) = \sum_{n=1}^{\infty} a_n \overline{y} K_{i\lambda}(2\pi n y) SC(2\pi n x);$$

where $K_\nu(x)$ is the K -Bessel function and $SC(x)$ is either $\sin(x)$ or $\cos(x)$. In the first case we say that f is "odd" and in the second f is "even." Furthermore, f is an eigenfunction of the Fricke involution

$$(2.2) \quad f(z) = f\left(\frac{1}{Nz}\right);$$

and f is also a simultaneous eigenfunction of the Hecke operators T_p for $p \nmid N$. A good introduction to this material is [4]. In this paper we only use the properties which are explicitly described above.

If $M \mid N$ then $\Gamma_0(N) \subset \Gamma_0(M)$. In particular, if $f(z)$ is a Maass form on $\Gamma_0(M)$ then $f(kz)$ is a Maass form on $\Gamma_0(N)$ for all $k \mid (N/M)$. Such functions are called "old forms" on $\Gamma_0(N)$ and it is natural to avoid such functions in a search for Maass forms, for they naturally belong on the larger group. The Maass forms which naturally live on $\Gamma_0(N)$, called "new forms", have a simple characterization in terms of their Fourier coefficients and we only search for new forms in our calculations.

In this paper we consider Maass forms on $\Gamma_0(p)$ for p prime. In this case there are four symmetry types: (even; +), (even; -), (odd; +), and (odd; -). For $p \leq 107$ we exhibit the first eigenvalue in each symmetry type, and we found the first 1000 new form eigenvalues on $\Gamma_0(11)$.

2.2. **Maass form L -functions.** We associate $f(z)$ to an L -function by the Mellin transform. If f is even then

$$(2.3) \quad L(s)G(s) = \int_0^\infty f(iy)y^s \frac{dy}{y^{\frac{3}{2}}};$$

where

$$L(s) = \sum_{n=1}^{\infty} \frac{a_n}{n^s}$$

is the associated L-function, and

$$(2.4) \quad G(s) = \int_0^{\infty} K_{iR}(y) y^s \frac{dy}{y} = 2^{s-2} \frac{s+iR}{2} \frac{s-iR}{2} :$$

Note that the series and integrals converge if $\Re(s)$ is sufficiently large.

If f is odd then

$$(2.5) \quad (2\pi)^{-s} L(s) G(s+1) = \int_0^{\infty} \frac{\partial f}{\partial x}(iy) y^{s-\frac{1}{2}} \frac{dy}{y};$$

with $L(s)$ and $G(s)$ as before.

The key properties of $L(s)$ are summarized in the following

Proposition 2.1. $L(s)$ continues to an entire function which satisfies the functional equation

$$(2.6) \quad \begin{aligned} L(s) &= N^{\frac{1}{4} + \frac{s}{2}} (2\pi)^{-s} L(s) G(s+a) \\ &= (1)^{s+1} (1-s); \end{aligned}$$

where $a = 0$ if f is even and $a = 1$ if f is odd, the ρ is determined by the eigenvalue of f under the Fricke involution and whether f is even or odd, and $G(s)$ is given in (2.4).

Proof. Let h equal f or $\partial f / \partial x$, depending on whether f is even or odd, respectively. Combining (2.3) or (2.5) with (2.2) we have

$$(2.7) \quad (2\pi)^{-s} L(s) G(s+a) = \int_0^{\infty} h(iy) y^{s-\frac{3}{2}+a} dy = (1)^s N^{\frac{1}{2}-s} \int_0^{\infty} h(iy) y^{s-\frac{1}{2}+a} dy$$

for any $\sigma > 0$. By (8.2) the above integrals converge for any value of s , which proves the analytic continuation. Set $\sigma = 1 - \frac{1}{N}$ to see that the right side satisfies the functional equation.

3. Locating Maass forms

The methods we use to locate Maass forms are similar to previous methods which have been used, such as that of Hejhal [3]. In this paper we only consider the case of $\Gamma_0(p)$, p prime, and furthermore we use the Fricke involution to separate symmetry types, so this means that we do not have to model vanishing at the cusps. Thus, except for the larger number of generators we can in principle use the exact same methods that have been used for Hecke triangle groups.

The following is a summary of the methods used to locate an individual Maass form. Given generators $fg_j g$ of Γ , we produce an overdetermined system of linear equations which uses a truncation of the Fourier expansion of f

$$f(z) = \sum_{j \in M} \sum_{m \neq 0} a_m K_{iR}(2\pi j y) \exp(2\pi i m x);$$

where the a_m are complex unknowns. Note that we assume $a_0 = 0$ (which excludes all Eisenstein series when we have only one cusp) and also normalize one of the coefficients (usually a_1) to equal 1. Also note that this of course depends on R (or equivalently on ρ). For most of the examples in this paper, we choose M so that the error caused by the truncation is around 10^{-8} for points in the fundamental domain of Γ .

We treat the $fa_n g$ as $4M - 2$ real unknowns. Next we choose N points z_i (where $N > 4M$) on a horizontal line in H . These points are mapped by the generators to points $g_j z_i = z_i$

higher up in H . If f is a Maass form on $H = \Gamma \backslash \mathbb{H}$ then $f(z_i) = f(z_1)$ (or more generally $f(z_i) = \chi(g_j) f(z_1)$ where χ is a character). The N equations

$$f(z_i) = \tilde{f}(z_i)$$

constitute an overdetermined system $Ax = b$ in $4M - 2$ unknowns. If R is an eigenvalue of a Maass form on $\Gamma \backslash \mathbb{H}$, then this system should be consistent to within the error caused by the truncation. Note: if one wishes to search only for new forms, then it is necessary to include additional equations to specify this. See [8].

Next we determine the least square solution x (using QR-factorization) to this system of equations. We then use the norm of the error, $\|Ax - b\|$, as a measure of how close R is to an eigenvalue. If R is really an eigenvalue, then $\|Ax - b\|$ should be roughly the size of the truncation error. In our initial calculations in cases where earlier data were available we found this to be true. We also found that away from eigenvalues (i.e. if we choose R randomly) the error is generally of size 1, independent of the size of the truncation error. We take $\|Ax - b\|$ to be a measure of distance between R and a "true" eigenvalue for $\Gamma \backslash \mathbb{H}$, and we have found this measure to vary smoothly and to be consistent with various other checks, which we describe below. Thus, it seems reasonable to say that these functions are a factor of 10^8 closer to being invariant under Γ than a randomly chosen function.

There are a number of error checks. If Γ is arithmetic then the Fourier coefficients will be multiplicative, and we find that the above method produces functions whose coefficients are multiplicative to better than the truncation error. These can be viewed as independent 1 in 10^8 error checks, which render it very likely that the functions produced are indeed Maass forms. In other words, the possibility of a "false alarm" is extremely small, and we have high confidence that the program is finding the Maass forms for Γ .

For nonarithmetic groups there are no Hecke relations, but there are other persuasive checks. We start with a general Fourier expansion with complex coefficients. For the Maass forms we find, the functions are real to very high accuracy (to an even higher accuracy than the truncation error). In general, when we are far from an eigenvalue, the system of equations is far from consistent and the approximate solutions are far from real.

A final check is the size of the Fourier coefficients. For arithmetic Γ all the coefficients we have found fit the Ramanujan-Petersen conjecture $a_p \ll p^{-1/2}$. For nonarithmetic groups that bound is not true in general, but it is still conjectured that $a_n \ll n^{-1/2}$. And we do in fact find that if R is close to an eigenvalue then the a_n from the least-squares solution are much smaller (and not growing as a function of n) than those from random R .

Our programs were implemented in Mathematica.

4. Low eigenvalues for $\Gamma_0(p)$

In Table 1 we present the first eigenvalue in each of the four symmetry types for $\Gamma_0(p)$, p prime.

Table 1 shows a few trends. For example, the first (even;+) eigenvalue tends to be smaller than the first (even;-) eigenvalue. This is not surprising because the number of nodal domains is an increasing function of the eigenvalue, and the symmetry relations force various constraints on the nodal curves. This also has an effect on the lower order terms in Weyl's law, which can be seen in Table 2.

To further study the low eigenvalues, we considered the normalized eigenvalues $\tilde{\lambda} = \frac{p+1}{12} \lambda$, where $\frac{p+1}{12}$ is the (reciprocal of the) coefficient of the leading term in Weyl's law, so that

| p | (even; +) | (even;) | (odd;) | (odd; +) |
|-----|-----------------|-----------------|-----------------|-----------------|
| 2 | 8.9228764869917 | 12.092994875078 | 7.220871975958 | 5.4173348068447 |
| 3 | 5.0987419087295 | 8.7782823935545 | 6.1205755330872 | 4.3880535632221 |
| 5 | 4.1324042150632 | 5.436180461416 | 4.897235015733 | 3.028376293066 |
| 7 | 3.454226503571 | 4.8280076684720 | 4.119009292925 | 1.924644305111 |
| 11 | 2.4835910595550 | 4.018069188221 | 2.96820576382 | 2.033090993855 |
| 13 | 2.025284395696 | 3.701627575242 | 2.8308066514473 | 0.97081541696 |
| 17 | 1.849687906031 | 3.169382380088 | 1.967986359638 | 1.441428545022 |
| 19 | 1.32979889046 | 3.0371960205 | 2.297006359074 | 1.09199155992 |
| 23 | 1.57958924015 | 2.61095996203 | 1.393337141483 | 1.5061266371 |
| 29 | 1.01726655080 | 2.35848525400 | 1.4875542669 | 1.21206072002 |
| 31 | 0.78935617774 | 2.3681029381 | 1.68678370214 | 1.06284037124 |
| 37 | 1.22324304054 | 2.07459336618 | 1.7095550812 | 0.6423059582 |
| 41 | 0.66572483212 | 2.00647646730 | 1.204395742494 | 0.86739746584 |
| 43 | 1.10814196343 | 1.80282682958 | 1.33429136841 | 0.65545238186 |
| 47 | 1.11157408467 | 1.6028012074 | 0.5854521430 | 1.2635566239 |
| 53 | 1.0158404282 | 1.49379571497 | 1.10150481917 | 0.8039894596 |
| 59 | 0.59582968816 | 1.7096938151 | 0.5985969867 | 1.0391204647 |
| 61 | 0.67704450723 | 1.7475722491 | 1.40716257846 | 0.41806231115 |
| 67 | 0.84247476 | 1.3611564746 | 1.0195601623 | 0.6775902092 |
| 71 | 0.3574504906 | 1.579666665 | 0.5829071706 | 1.02176122015 |
| 73 | 0.654548913 | 1.402091810 | 1.3304765833 | 0.5178875052 |
| 79 | 0.5517748428 | 1.5496128514 | 0.9963893608 | 0.7490008694 |
| 83 | 0.817132725 | 1.0975181181 | 0.6402875784 | 0.95188877503 |
| 89 | 0.489435980 | 1.4372631258 | 0.860333981 | 0.688804233 |
| 91 | 0.6038860327 | 1.206246429 | 1.132502360 | 0.416931671 |
| 101 | 0.453759608 | 1.30563134 | 0.546229605 | 0.77990698 |
| 103 | 0.685190643 | 1.08157342 | 0.724051309 | 0.56540244 |
| 107 | 0.840011226 | 0.90440769 | 0.581677094 | 0.90574018 |

Table 1. First eigenvalue, R , in each of the four symmetry types of $\chi_0(p)$, for prime $p \leq 107$. Values shown are truncations of the actual values, and all digits are believed to be correct.

$\tilde{\lambda}_n$ for the n th eigenvalue. Figure 1 shows the cumulative distribution functions of the first $\tilde{\lambda}_n$ in each symmetry type. If each symmetry type was equally likely to have the lowest eigenvalue then each plot would correspond to a p.d.f with mean 4. This is not the case, for the reasons described in the previous paragraph. A more sophisticated normalization, involving the lower order terms in Weyl's law, would be needed in order to reveal any underlying structure.

5. The first 1000 Maass forms on $\chi_0(11)$

We applied the method described in the previous section to find all Maass new forms on $\chi_0(11)$ with $R < 36.5$, resulting in a total of 1054 eigenvalues. The first 30 eigenvalues in each symmetry type are given in Table 2.

5.1. Weyl's law justification that the list is complete. It is natural to question whether our list of 1000 eigenvalues is complete. It is possible to do a calculation using the trace formula to justify this assertion, as in [2]. However, we will use a simpler but less rigorous

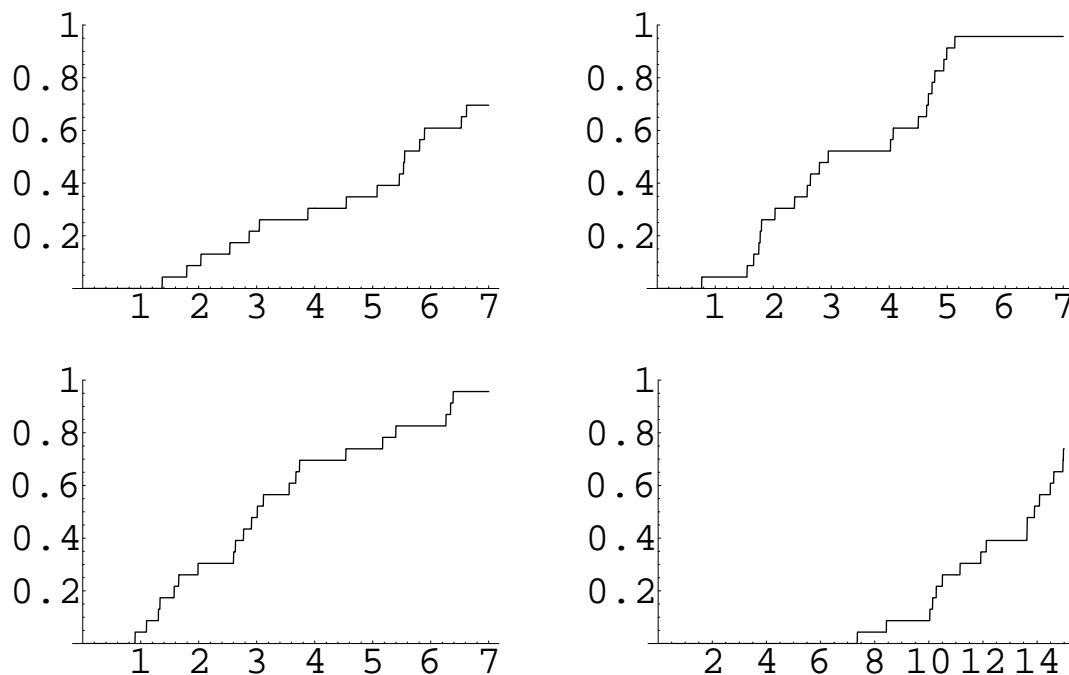


Figure 1. Cumulative distributions of the rescaled first eigenvalue in each of the four symmetry types for $\rho_0(p)$. Clockwise from top right we have even plus, even minus, odd minus, and odd plus.

method involving Weyl's law. This approach is well known to physicists and we do not claim that any of the ideas in this section are new.

The method we describe is quite robust and does not require any a priori knowledge about the eigenvalue counting function. In addition to checking lists of eigenvalues, the method also works well for zeros of L-functions, zeros of derivatives of L-functions, and no doubt many other cases. In some of these cases we know very precise information about the counting function of the objects being studied, but this is not necessary for the method.

Let $N(x) = \#\{f_j : 0 < f_j \leq x\}$. The method is based on the assumption that there exists a nice function f , which is of a fairly simple form, such that

$$(5.1) \quad r(x) = N(x) - f(x)$$

grows very slowly and averages to 0 over small intervals. Weyl's law provides the leading order behavior of $f(x)$, and in many cases some lower order terms are known, but we do not claim that one can prove that the list of eigenvalues is complete only by using established facts about Weyl's law.

We justify that our list of eigenvalues is complete in two steps:

- demonstrate that the function f exists for our claimed complete list of eigenvalues.
- demonstrate that the function f does not exist for lists with missing eigenvalues.

First we consider the case of all new forms on $\rho_0(11)$, and we assume that the function f has the form $f(x) = Ax + B\sqrt{x}$. If we choose A and B to give the best least-squares fit we find $A = 0.83305$ and $B = 1.51762$. This shows good agreement with the known main

| (even; +) | (even;) | (odd;) | (odd; +) |
|---------------|---------------|---------------|---------------|
| 2.48359105931 | 4.01806918817 | 2.03309099399 | 2.96820576406 |
| 3.28347243577 | 4.55526078519 | 3.03251283477 | 3.67969872541 |
| 4.71167698688 | 5.763876683 | 3.48188847623 | 4.52889442543 |
| 4.93319801514 | 6.24170090061 | 4.47950391861 | 5.38428160742 |
| 5.26506649404 | 6.50705758603 | 4.73801386035 | 5.86853222013 |
| 5.98954160832 | 7.16536040411 | 4.96681056818 | 6.03361084498 |
| 6.53884437369 | 7.73368897382 | 5.66326548842 | 6.77549239897 |
| 6.61367515372 | 7.88007383371 | 6.06921835945 | 7.02463370057 |
| 7.26644184877 | 8.62006794999 | 6.58162198432 | 7.59926619568 |
| 7.57048468847 | 8.99092809554 | 6.83944314323 | 7.68091057664 |
| 8.1420217952 | 9.10172820901 | 7.29898901659 | 8.43825975028 |
| 8.2745067789 | 9.22640277057 | 7.48914848604 | 8.55580430772 |
| 8.51378467778 | 9.58661569223 | 7.51799881213 | 8.57197306999 |
| 8.67868612906 | 10.1232769351 | 8.04940484112 | 9.04133195689 |
| 9.34515203418 | 10.3790777119 | 8.16066289206 | 9.46659932758 |
| 9.58209996953 | 10.6466817416 | 8.65213300992 | 9.58865618615 |
| 9.67447022214 | 10.9372887384 | 8.92993868939 | 10.1617823366 |
| 9.86213636813 | 11.1472353004 | 9.19975228208 | 10.2760011943 |
| 9.98570867995 | 11.4784159679 | 9.67408869747 | 10.6445164137 |
| 10.6430998724 | 11.785015526 | 9.70588526636 | 10.6694194813 |
| 10.6895930795 | 11.8109636758 | 9.85493309024 | 10.989904792 |
| 11.1502516477 | 12.0601741852 | 10.1854915198 | 11.2612425027 |
| 11.1780820772 | 12.6105517277 | 10.3386794422 | 11.2733375812 |
| 11.4741161917 | 12.6118028204 | 10.5313292208 | 11.8005163423 |
| 11.6836999337 | 12.9273387317 | 10.8165867701 | 11.8348731714 |
| 11.9293065449 | 12.9741004148 | 10.9051400611 | 11.9611740135 |
| 12.038113214 | 13.1014471689 | 11.3280653248 | 12.2747697039 |
| 12.3049680989 | 13.3464693158 | 11.5395912507 | 12.6217030476 |
| 12.5345178216 | 13.9313207377 | 11.6712226728 | 12.8306123388 |
| 12.6348846255 | 13.9973467855 | 11.7801194448 | 13.0161442996 |

Table 2. First 30 newform eigenvalues in each symmetry type of $\rho_0(11)$. Values shown are truncations of the actual values, and all digits are believed to be correct. Note that there are only three oldforms in the range covered by the table: an even oldform at $R = 13:779751$, and odd oldforms at $R = 9:533695$ and $R = 12:173008$.

term of $A = 10 = 12 \cdot 0.83333$. Figure 2 plots the function $r(x)$, as well as $r(x)$ averaged over a moving window of width 150.

As can be seen, the function $r(x)$ is small, and it is also small on average.

We now repeat the calculation on a list of eigenvalues which is known to be incomplete, to demonstrate how the method detects the missing value. In Figure 3 we consider the eigenvalues in the (even, \quad) space, for which we have removed one eigenvalue 510. Since we are in the (even, \quad) space, there are only $1/4$ as many eigenvalues, so it should actually be easier to fit a main term function $f(x)$. We want to make the point that it is impossible to find functions f and r for this list of data. We choose f of the form

$$(5.2) \quad f(x) = Ax + B \frac{P}{x} \log x + C \frac{P}{x} + D x^{\frac{1}{4}} + E \log x + F;$$

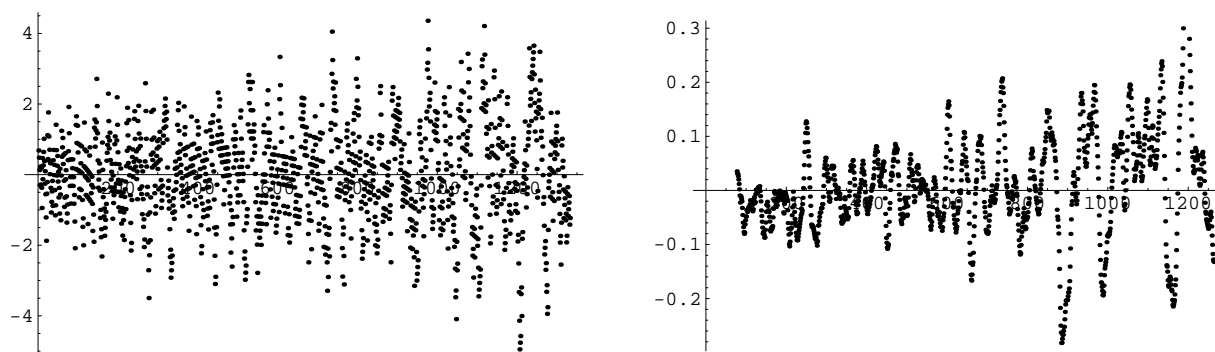


Figure 2. The remainder function $r(x)$ defined in (5.1) where $f(x)$ is chosen as described in the text. The data is the 1054 new forms on $\mathbb{F}_0(11)$ with $x < 1260$. The plot on the right is the running average over a window of length 150.

and then choose $A; B; C; D; E; F$ to give the best least-squares fit. The resulting $r(x)$ and $r(x)$ averaged over a window of size 150 is shown in Figure 3.

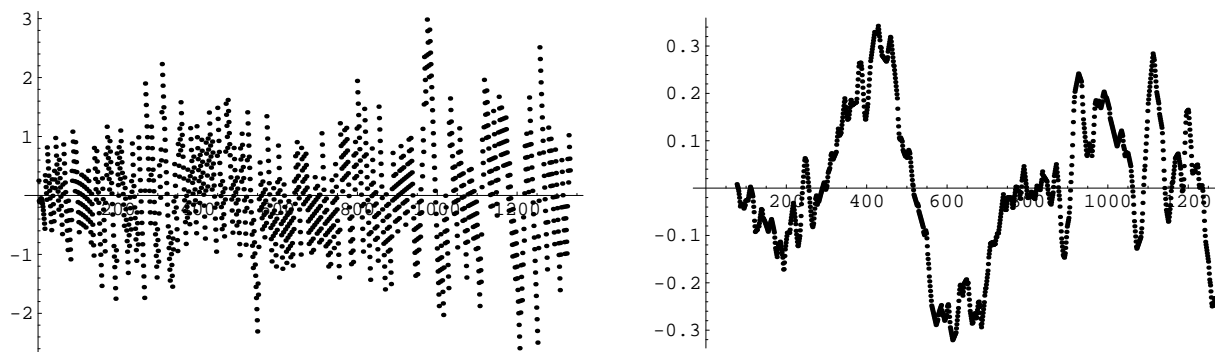


Figure 3. The remainder function $r(x)$ for the first 250 (even,) new form eigenvalues on $\mathbb{F}_0(11)$, where one eigenvalue with $R^2 = 510$ has been intentionally omitted. The plot on the right is the running average over a window of length 150.

As can be seen, $r(x)$ does not average to zero over small intervals, and in fact we can almost read off the missing value 510 from the averaged graph. The fact that we fit a function with many free parameters is meant to suggest the robustness of the method. Unfortunately, when fitting such a general function to such a small amount of data, we can no longer use the coefficient A of the main term to check the known main term in Weyl's law.

5.2. Shortcomings of the method. There are some obvious shortcomings of the method of fitting Weyl's law to check the data.

First, the method cannot detect missing eigenvalues at the beginning of the list. Such missing terms are absorbed by the constant term in our function.

Second, if a large number of eigenvalues are missing, and the missing eigenvalues are very regularly spaced, then this may not be detected. Indeed, that is exactly the situation at hand. We are claiming to demonstrate that our list of new form eigenvalues is complete.

But if we were mistakenly claiming that we had the list of all eigenvalues, that error would not be immediately caught by our test to "Weyl's law," for the missing eigenvalues, i.e. the oldforms, are regularly spaced. Indeed, they have their own Weyl's law. In the case here, we know the coefficient of the main term in the counting function for new forms, and our test function shows good agreement with that. However, we cannot rule out the possibility that we are systematically missing every 100th eigenvalue, for example.

5.3. Statistics of the eigenvalues. It is generally believed that the new form eigenvalues in each symmetry class are as uncorrelated as possible (have Poisson statistics), the new form eigenvalues in the different symmetry classes are uncorrelated, and there is no correlation between new form eigenvalues and oldform eigenvalues. For the case of $SL(2;Z)$ these conjectures are strongly supported by numerical evidence [3]. We now check if our data supports these conjectures. Only the case of the spacing of oldforms within the list of new forms can be considered new here.

In Figure 4 we consider the nearest neighbor spacing of the eigenvalues on $\Gamma_0(11)$, both for the full spectrum and for one particular symmetry type. Good agreement with Poisson statistics is found.

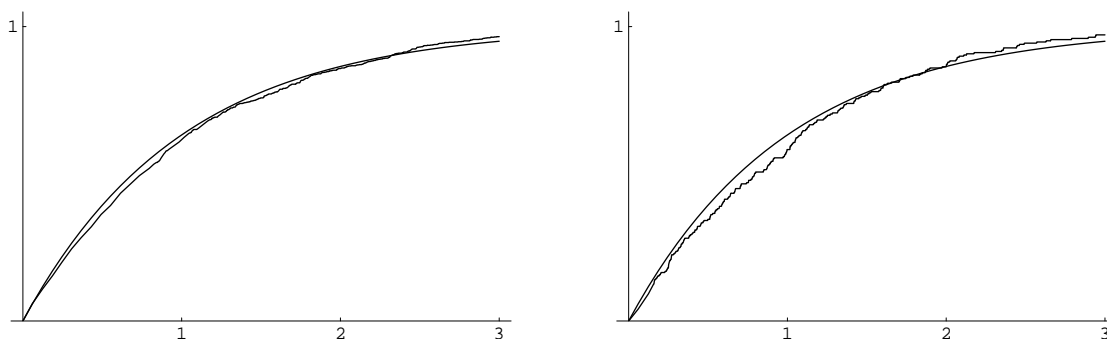


Figure 4. Cumulative distribution of normalized nearest neighbor spacing of new forms on $\Gamma_0(11)$. The smooth curve is the cumulative distribution for Poisson spacing. The plot on the left is for all new forms and the plot on the right is for (even,) forms.

Next we consider the location of the oldforms among the new forms. If there is no correlation then the oldforms should be distributed uniformly between the two neighboring new forms. Figure 5 shows the (scaled) location of the oldforms between the neighboring new forms, giving a good agreement with the expected Poisson distribution.

6. Example Maass L-functions

We give example plots of Maass L-functions and discuss some general features, and in the next section we consider the statistics of zeros and critical values.

By the functional equation, $L(\frac{1}{2} + it)$ is real for real t , so there is a simple rescaling (involving a ratio of ζ -functions) to produce a function with the same modulus as $L(\frac{1}{2} + it)$ which is real for real t . It is that real function of the real variable t , which we still call "the L-function", which is shown in Figure 6. There are four classes of L-functions, depending on whether the function f is even or odd as a function of x , and whether f has eigenvalue $+1$ or -1 under the Fricke involution. One example of each combination is shown in Figure 6.

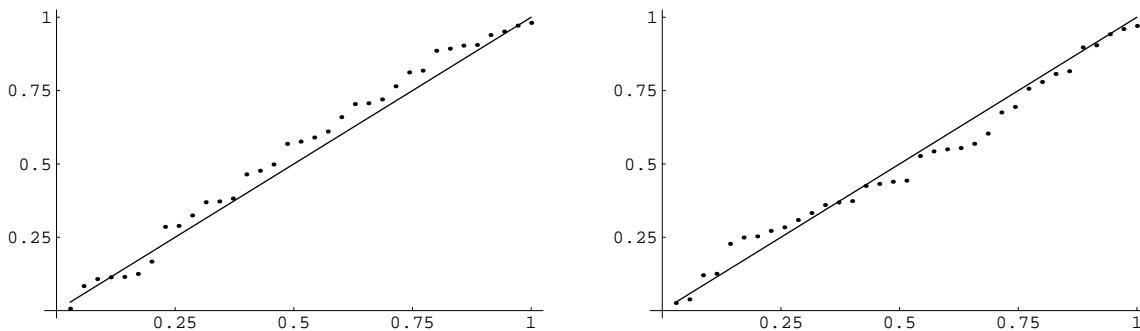


Figure 5. Ordered normalized location of odd oldforms within neighboring newforms, for the 35 oldforms with $R < 36.5$. Straight line is comparison to random (Poisson) spacing. The plot on the left is for odd, on the right for odd+.

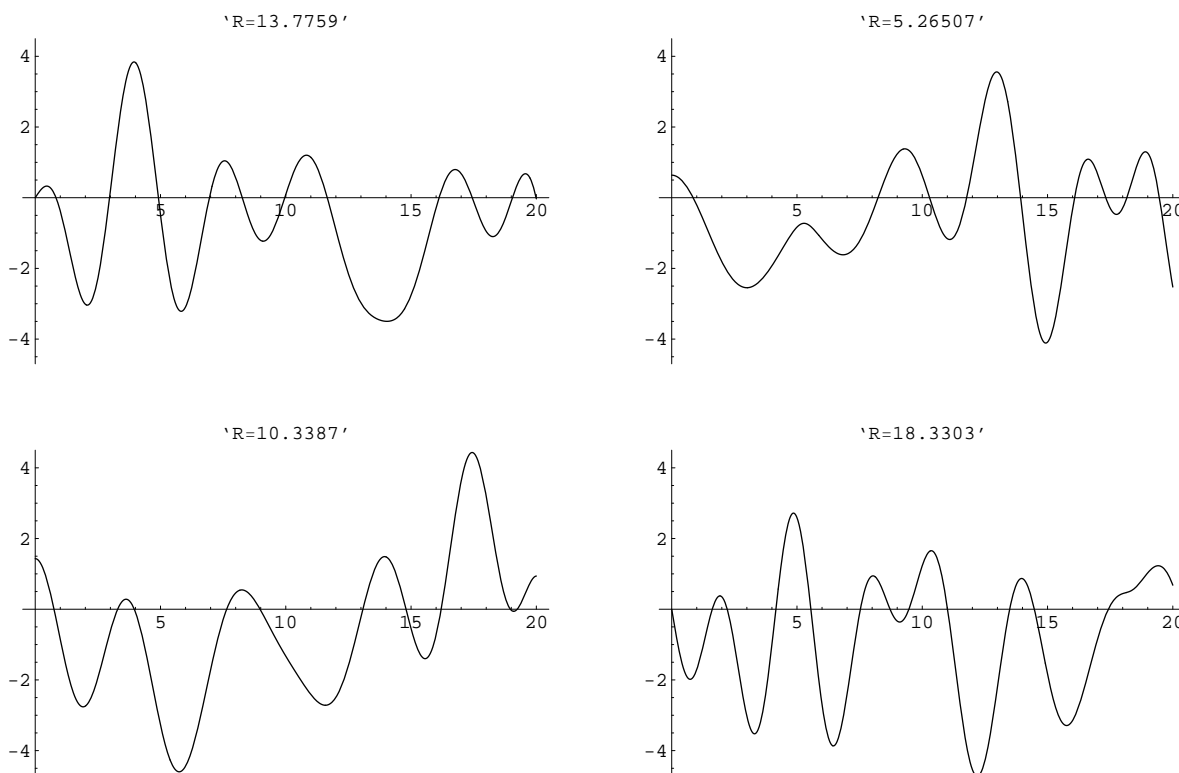


Figure 6. Plots of (the real version of) $L(\frac{1}{2} + it)$, one for each of the four symmetry types of Mass forms on $\rho_0(11)$. Clockwise from top right we have odd plus, even plus, even minus, and odd minus. Each plot is labeled with the "eigenvalue" R of the Mass form.

The first thing to notice is that these plots make it appear that the Riemann hypothesis is false for these L-functions. For example, in the upper-right plot, the negative local maximum near $t = 5$ indicates a zero on the critical line. However, that zero on the line is a trivial zero, which has imaginary part iR , so this is not a counterexample to the Riemann Hypothesis.

The effect of the trivial zeros is more noticeable in the even case, where they are closer to the critical line. This illustrates Strombergsson's [9] observation of a gap in critical zeros near $t = R$.

The average spacing of zeros is a function of both R and t , the precise dependence can be deduced from the functional equation and the argument principle. For our purposes it suffices to note that for $|t| < R$ the zero spacing is primarily a function of R , increasing with R , except for a slight decrease in density near $|t| = R$.

The number $\epsilon = (-1)^{j+1}$ from (2.6) is called "the sign of the functional equation." If $\epsilon = +1$ then $L(\frac{1}{2}) \neq 0$, and we call $L(\frac{1}{2})$ the "critical value". If $\epsilon = -1$ then $L(\frac{1}{2}) = 0$ and $L^0(\frac{1}{2})$ is the critical value.

7. Checking the random matrix predictions

Random Matrix Theory has become a fundamental tool for understanding the zeros of L-functions. Montgomery [6] showed that (in a limited range) the two-point correlations between the non-trivial zeros of the Riemann ζ -function is the same as that of the eigenvalues of large random unitary matrices, and he conjectured that the correlation we in fact equal. There is extensive numerical evidence [7] in support of this conjecture, and in particular many statistics of the zeros of the ζ -function, such as the distribution of nearest neighbor spacing, are believed to be the same as that of large random unitary matrices. Katz and Sarnak [5] introduced the idea of studying zero distributions within families of L-functions and have conjectured that these coincide with the eigenvalue distributions of the classical compact groups: unitary, symplectic, and orthogonal. For these groups the bulk of the eigenvalue distributions are the same, it is the eigenvalues near 1 which have different distributions in each case. In terms of L-functions this corresponds to zeros near the critical point, so our concern is with the low lying zeros.

The family of Maass L-functions is an Orthogonal family (see [1]), which we further break into $O^+ = SO$ (even) and $O^- = SO$ (odd), depending on whether the L-function has sign $+1$ or -1 in its functional equation. In the latter case $L(\frac{1}{2}) = 0$, which corresponds to the fact that odd orthogonal matrices have 1 as an eigenvalue.

In Figure 7 we consider the distribution of the height of the first zero above the critical point, comparing to the analogous quantity for eigenvalues of orthogonal matrices. In Figure 7 we omit the Maass forms with $R < 15$, because the small values of R cause anomalous behavior of the first few zeros.

Next we show the cumulative distribution of the critical values, t to the prediction from random matrix theory. In the case of even functional equation, corresponding to O^+ matrices, the density of critical values scales as $c^0 \bar{x}$ for small x . This is quite difficult to see in a histogram, so instead we consider the cumulative distribution and compare to the predicted $c^0 \bar{x}$, where we choose c^0 by fitting to the data. Figure 8 shows very good agreement.

In Figure 8 we omit the first 30 Maass forms of each symmetry type, corresponding to approximately $R < 13$, because the small values of R cause anomalous behavior near the critical point.

In the case of odd functional equation, $\epsilon = -1$, the density of small values is predicted to scale as $c^0 x^{3/2}$. In particular, there should be very few small values. Indeed we find very few cases where $L^0(\frac{1}{2})$ is small, but our statistics are too low to make a meaningful comparison with the random matrix prediction.

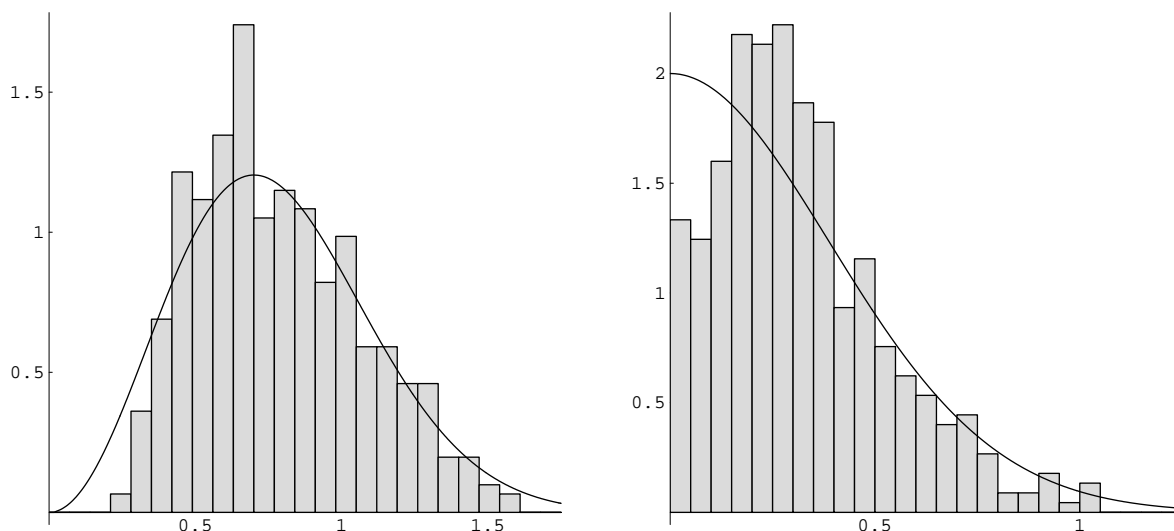


Figure 7. Density of first zero above the critical point for 435 L-functions with $\chi^2 = -1$ on the left, and 450 with $\chi^2 = +1$ on the right. The continuous curves are the densities for the corresponding eigenvalues for O^- and O^+ , respectively. The L-function zeros have been rescaled to have the same averages as the corresponding eigenvalues.

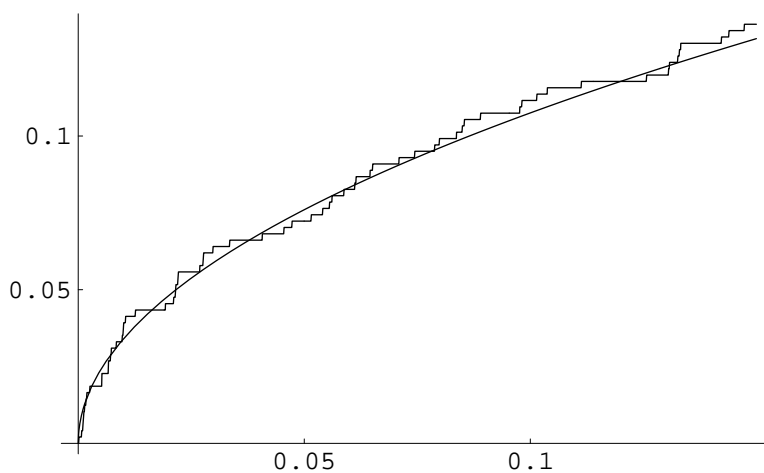


Figure 8. Cumulative distribution of critical values for $\chi^2 = +1$ L-functions. A total of 484 L-functions were considered, of which 63 feature in this plot. The continuous curve is $0.34\sqrt{x}$.

Finally, we show the distribution of nearest neighbor spacings. In Figure 9 we consider Mass forms with $R > 21.5$, and we considered the neighbor gaps between zeros starting with the 5th zero and going up to $t = 20$. This was designed to avoid the anomalous behavior near the critical point and near $t = R$. In addition we rescale the zeros to remove the trend of decreasing spacing with increasing R and t . The fit to the random matrix prediction in Figure 9 is quite good. Indeed this may be somewhat surprising because the zeros considered

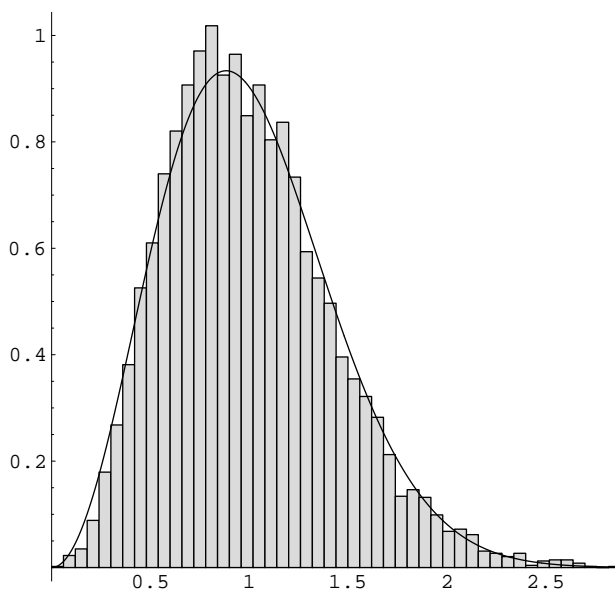


Figure 9. Nearest neighbor gaps, normalized to remove the dependence on R and t . A total of 8086 neighbor gaps from approximately 650 L -functions. The continuous curve is the normalized nearest neighbor spacing of eigenvalues of large random unitary matrices.

there lie in the range $t_j < R$, which one might expect to be different from the $t \rightarrow 1$ case. Perhaps this illustrates the universality of the random matrix behavior.

8. Computing $L(s)$

Our interest is in the low-lying zeros of $L(s)$, so we only require an efficient method of evaluating $L(s + it)$ for small t .

Substituting (2.1) in to (2.7), and then switching the order of summation and integration, we have

$$\begin{aligned}
 (2^{-s})^s L(s) G(s+a) &= (2^{-s})^{(2a-1)(s)} \prod_{n=1}^{\infty} a_n n^{(2a-1)(s)} \int_0^1 K_{iR}(y) y^{s+(a-1)} dy \\
 &\quad (1)^{a-1} N^{\frac{1}{2}-s} (2^{-s})^{(1-s)(2a-1)} \prod_{n=1}^{\infty} a_n n^{(1-s)(2a-1)} \int_0^1 K_{iR}(y) y^{a-s} dy \\
 &= (2^{-s})^s \prod_{m=1}^{\infty} X^m \prod_{n=1}^{\infty} a_n n^{-s} \int_0^1 K_{iR}(y) y^{s-1+a} dy \\
 (8.1) \quad &\quad (1)^{a-1} N^{\frac{1}{2}-s} (2^{-s})^{s-1} \prod_{m=1}^{\infty} X^m \prod_{n=1}^{\infty} a_n n^{s-1} \int_0^1 K_{iR}(y) y^{a-s} dy
 \end{aligned}$$

We use the above expression, truncating the sum over m , in our calculations.

To decide where to truncate the sum, we use the estimate

$$(8.2) \quad K_{iR}(y) \sim \frac{r}{2y} e^{-y \frac{R}{2}};$$

for $y > 2R$. We also must assume a bound on the coefficients a_n . It is conjectured that $\sum_{j|n} j^{-d(n)}$, where $d(n)$ is the number of divisors of n . That bound is far from being proven, but since it holds for all coefficients which have been computed, we assume it in our estimates. Finally, to isolate $L(s)$ we must divide the above expression by $(2 - \epsilon)^s G(s + a)$. This increases the required precision because $G(s)$ decays rapidly as s increases. However, this will not be an issue because our concern is with low-lying zeros.

The Bessel function $K_{\text{ir}}(y)$ oscillates rapidly as $y \rightarrow 0$, so it is desirable to have the lower limit of integration as high as possible. This is accomplished by choosing $\epsilon = 1 - \frac{1}{N}$. Since ϵ is a free variable, we implemented an error check that looks for differences in $L(s)$ when different values of ϵ are used, finding good agreement.

We used the above considerations to produce L -functions values with an error of approximately 10^{-6} , for t up to m in $(20; R)$. Since we only seek data to produce statistics involving neighbor spacing and value distributions, this level of accuracy is more than adequate. If one wanted to study many zeros of a single L -function then more sophisticated methods would be needed.

References

- [1] J.B. Conrey, D.W. Farmer, J. Keating, M. Rubinstein, and N.C. Snaith, "Integral moments of L -functions", to appear in *PLMS*, arxiv.org/abs/math/0206018.
- [2] A. Booker, A. Strombergsson, A. Venkatesh, Effective Computation of Mass Cusp Forms, preprint.
- [3] Hejhal, Dennis A. Eigenvalues of the Laplacian for Hecke triangle groups. *Mem. Am. Math. Soc.* 97 (1992), no. 469, vi+165 pp.
- [4] Iwaniec, Henryk, Spectral methods of automorphic forms. Second edition. Graduate Studies in Mathematics, 53. American Mathematical Society, Providence, RI; Revista Matemática Iberoamericana, Madrid, 2002.
- [5] N.M. Katz and P. Samak, Random matrices, Frobenius eigenvalues, and monodromy, *AMS Colloquium Publications*, 45 *AMS*, Providence, RI 1999.
- [6] H.L. Montgomery, The pair correlation of zeros of the Riemann zeta-function, *Proc. Sympos. Pure Math.* 24 1973 pp. 181-93.
- [7] A. Odlyzko, The 10^{20} th zero of the Riemann zeta-function and 70 million of its neighbors., Preprint 1989.
- [8] Rankin, Robert A. Modular forms and functions. Cambridge University Press, Cambridge-New York-Melbourne, 1977.
- [9] A. Strombergsson, On the Zeros of L -Functions Associated to Mass Waveforms *International Mathematics Research Notices*, 15 1999, 839{851

American Institute of Mathematics
 360 Portage Ave.
 Palo Alto, CA 94306
 farmer@aimath.org

Chalmers University of Technology,
 SE-412 96
 Goteborg, Sweden
 sj@math.chalmers.se